Anticancer, Antioxidant Activities and Molecular Docking Study of Thiazolidine -4-one and Thiadiazol Derivatives

Tahseen Abdul qader Alsalim (tahseen.alsalim@uobasrah.edu.iq)
University of Basrah College of Education for Pure Sciences https://orcid.org/0000-0002-4838-511X
Noor M. Nasir
University of Basrah College of Education for Pure Sciences
Amr Ahmed El-Arabey
Al-Azhar University Faculty of Medicine
Mohnad Abdalla
Shandong University School of Chemistry and Chemical Engineering

Research Article

Keywords: HepG-2, Thaiazolidinone, AKT1, CDK4, Apoptosis, Cell cycle, Immunomodulation

Posted Date: January 3rd, 2022

DOI: https://doi.org/10.21203/rs.3.rs-1200559/v1

Abstract

Liver cancer accounts for a major portion of the global cancer burden. In many nations, the prevalence of this condition has risen in recent decades. New series of thaiazolidinones and thaiadiazolidine have been designed, synthesized, and evaluated for potential antioxidant and antihepatocarcinogenic activity. The antioxidant activity of synthesized compounds was evaluated using a DPPH assay. Furthermore, we examined the compounds against HepG2 cells using MTT assay, flow cytometry analysis through the cell cycle, reactive oxygen species, and apoptosis. The result showed that compound 6b has the highest antioxidant activity with IC_{50} =60.614±0.739 μM. The anticancer activity showed that compounds 5 and 6b have significant toxicity against liver cancer cells HepG2, IC50 values (9.082 and 4.712) μM, respectively. Flow cytometry experiments revealed that compound 5 arrested HepG2 cells in the S process, while compound 6b arrested HepG2 cells in the G1. Compound 6b had a greater reduction in reactive oxygen species and late apoptosis than compound 5. Substantially, compound 5 had affinity energies of -7.6 and -8.5 for Akt and CDK4 proteins, respectively, but compound 6b had affinity energies of -7.8 and -10.1 for Akt1 and CDK4 proteins, respectively. Consequently, compound 6b had lower binding energies than compound 5. In this work, we used multiple bioinformatics methods to shed light on the prospective therapeutic use of these series as novel candidates to target immune cells in the tumor microenvironment of hepatocellular carcinomas such as CD8+ T cells, endothelial cells, and hematopoietic stem cells. The results of antioxidant, anticancer, molecular docking studies, and bioinformatic analysis showed that compound 6b has a potential impact and could be developed for drug discovery with further research.

1. Introduction

The incidence of cancer is increasing, according to the annual report of the Health Organization, as there are millions of new cases [1]. Since 1980, the incidence of liver cancer has more than quadrupled, while the mortality rate has more than doubled. In the United States, there are expected to be 42,230 new cases and 30,230 deaths from liver cancer in 2021(https://www.cancer.org). Liver hepatocellular carcinoma (LIHC) is fatal cancer with no viable therapy. The Cyclin-dependent kinases 4/6 (CDK4/6) and PI3K/AKT signaling pathways are important in carcinogenesis and offer prospective therapeutic options for LIHC[2]. Akt1 ablation has been shown in genetic research in mice to significantly reduce hepatic carcinogenesis. In terms of Akt1, a 2019 study found that Akt1-mediated phosphorylation of mTORC2 is critical for starting hepatocarcinogenesis in humans and animals, as it activates c-Myc, thus promoting cellular growth [3]. Strong evidence suggests that CDK4 is a clinical prognostic marker for LIHC patients[4]. As a result, the development of novel potential medicines targeting AKT1 and CDK4 may represent an unmet medical need. Tumor microenvironment (TME) is a dynamic biological environment surrounded by tumors that include macrophages, stroma, fibroblasts, dendritic cells, stem cells, lymphocytes, pericytes, adipocytes, and blood vessels[5]. However, no studies on the connection between AKT1 and CDK4 and invading immune cells in the TME have been undertaken.

Heterocyclic compounds have medicinal uses, considered as privileged scaffolds in the discovery of drugs[6]. The researchers try to find new ways to design and synthesize new derivatives of heterocyclic compounds [7]. Sulfur-containing substances such as 1,3,4-thiadiazolines and thaiazolidinone have received great attention from medicinal chemists due to their biological activities and remarkable pharmacological properties and there are commercial drugs such as methazolamide acetazolamide and etozoline[8–10]. 1,3,4-thiadiazole and thaiazolidinone are the best heterocyclic compounds that have a wide spectrum of biological activity. Such as activity an antibacterial, antifungal[11–13], anti-HIV-1, inhibitors of cancer and central nervous system (CNS) [14–21]. And have a strong biological activity, therefore widely used in the pharmaceutical, medicinally, and as pesticides[22–24]. Therefore, for the synthesis of new 1,3,4-thiadiazolines and thaiazolidinone derivatives, there are several methods to obtain 1,3,4-thiadiazoles, mostly achieved by condensation substituted thiohydrazide with thiocyanate, also by the reaction between thiosemicarbazone with acetic anhydride [25–29]. The heterocyclic thaiazolidinone is mostly achieved by the reaction from the reaction isomethan group with thioglycolic acid [30], also a reaction chloroacetic acid with thiosemicarbazones[31–33].

Given these findings, the current study's goal is to synthesize thaiazolidinone and thaiadaiazoline derivatives. The synthesized heterocyclic compounds were characterized using spectroscopic methods such as IR, 13C, 1H NMR, and mass spectroscopy. They were then evaluated as antioxidants, anticancer (HepG-2), molecular docking studies of a target protein Akt1, and CDK4, and bioinformatic analysis of immune cell infiltration in the TME of LIHC patients.

2. Result And Discussion

2.1. Antioxidant potential

For many living things, oxidation is necessary for the production of energy [34]. However, the continually generated free radical reactive oxygen (ROS) species may destructively cause RNA, DNA, causing mutations, chromosomal damage, and the oxidation of unsaturated fatty acids. ROS promotes heart disease, neurological disease, cancer, and aging, and contributes to enhancing oxidative damage[35]. However, antioxidants help protect the body from free radical damage and are necessary for the human body to scavenge the radicals are produced from mitochondria leak, pollution, sunlight, ultraviolet ray, and smoking [36].

Several antioxidant scans are collected under the subject of HAT or single electron transfer (SET). The DPPH concentration reduce with time and change in color from purple to yellow and/or colorless owing to the transfer of the atomic hydrogen, was used in the measurements of scavenging activity of studied compounds (2,3a,3b, 3c, 3d, 3e, 4, 6a, and 6b) at concentrations of 50, 75, 100, and 200 μM. At a concentration of 200 μM, the inhibition activity was (9.02% – 77.778%). The inhibition activity percentage of all studied compounds is shown in Figure 1 and data were collected in Table 1.

Table 1
In-*vitro* antioxidant inhibition activities of compounds (**2,3a,3b, 3c, 3d, 3e, 4, 6a**, and **6b**).

Compounds	Concentration				IC_{50}
	50 µM	75 µM	100 µM	200 µM	
2	35.817	45.686	48.954	60.392	105.56023 ± 4.4564
3a	19.497	29.379	32.026	39.673	=
3b	19.15	24.281	30.033	34.314	=
3c	7.68	14.183	15.686	14.371	=
3d	8.072	18.431	18.954	20.261	=
3e	6.34	10.131	18.987	18.954	=
4	4.837	6.892	8.17	9.02	=
6a	47.582	56.699	65.817	77.778	55.75931 ± 0.2850
6b	45.261	53.987	65.359	75.98	60.61429 ±0.7391

Several antioxidant scans are gathered under the topic of hydrogen atom transfer (HAT) or single electron transfer (SET). Their action can be clarified through the oxidative mechanism of phenolic antioxidants. The values of the scavenging activity of the synthesized compounds (2,3a,3b, 3c, 3d, 3e, 4, 6a, and 6b) at concentrations 50, 75, 100, and 200 µM, were measured by the decrease of DPPH absorbance at 517 nm with time and the change of the DPPH color from purple to yellow or colorless due to the transfer of hydrogen atom. The inhibition activity at a concentration of 200µM within the range (9.02% – 77.778%), the inhibition percentage activity of the studied compounds shows in figure 1, and data was gathered in Table 1.

The inhibitions activity of compounds 6a, 6b, and 2 were quite high (200 µM) in DPPH. While the other compounds exhibited less inhibitory activity of DPPH, due to for absence of the phenolic OH group, which provided the 6a, 6b, and 2 compounds with a strong radical activity of scavenging by giving radicals of DPPH hydrogen atom and inhibiting radical activity with HAT[37]. Consequently, the radical scavenging activity of compounds 6a, 6b, and 2 were in the order: 6a> 6b>.2>

The half-maximal inhibitory concentration (IC50) for the studied compounds was calculated by GraphPad Prism 8.02. The IC_{50} inhibition of 6a, 6b, and 2 compounds was 55.729 ± 0.285, 60.614±0.719, and 105.56 ± 4.456 µM respectively. The results showed that the IC_{50} values are consistent with the inhibition activity and that compounds with a phenolic group can scavenge free radicals and inhibit the oxidizing agents via the transfer of hydrogen atomic (HATs). So the most efficient which have phenolic groups were the most efficient as an antioxidant to the radical source.

2.2. Anticancer activity

Liver cancer is one of the most common malignant tumors in the world[38]. The fast growth in liver cancer incidence, lack of adequate treatment have led us to look for new and more efficient molecules[39].

Because of the action of the thaiazolidinone and thaiadaiazoline rings, as well as their ability to communicate with biological targets, they have a variety of biological applications, including antimicrobial and antitumor [40, 41]. As a result, it may be a starting point for developing new anticancer agents. We tested five new thaiazolidinone and thaiadaiazoline derivatives against liver cancer cells in this study (HepG2). The compounds had varying anticancer activity against the HepG2 cell line, figure (2) shows the IC_{50} values within the range (4.712-46.60) μM. The studied compounds were taken from the lowest IC_{50}. Compound 6b has the lowest IC50 value of 4.712 μM, compound 5 with IC_{50} value of 9.082 μM, compound 2 with IC50 17.49 μM and compound 4 and 6a has IC_{50} value 38.616 μM and 46.60 μM respectively and The results showed substantial anti-cancer efficacy against the HepG2 cell line of the investigated substances. Therefore compounds 5 and 6b which has the lowest IC_{50} being used in subsequent flow cytometry experiments (cell cycle, reactive oxygen species, and apoptosis). The IC_{50} values of compounds 5 and 6b were used in cell cycle phase detection, with compound 5 arresting cells in the S phase (Figure 3, B2) and compound 6b arresting cells in the G1 phase (Figure 3, B3), as compared to the monitor (Figure 3, B1). Figure 4 depicted the impact of compounds 5 and 6b on reactive oxygen species, DCFH+ for the control was 90.8%, which was increased to 92.8% by using the IC50 value of compound 5, and raised to 96.0% by using the IC50 value of compound 6b. This increase in DCFH ratio compared to the control revealed that compound 6b has a greater impact on HepG2 cells than compound 5, which was improved by the apoptosis experiment. Figure 3(A) shows that the IC50 value of compound 5 has a late apoptosis ratio (Q2) of about 15.1%, compared to the control late apoptosis ratio of 42.1%, and compound 6b increased the late apoptosis ratio to 19.6% when compared to live cells (Q4). Therefore, these results suggest that compounds 5 and 6b are potential cytotoxic agents. One reason for apoptosis might be the observed capacity of compounds to cause cell cycle arrest. The principal regulatory mechanisms for cell growth and proliferation are known as cell cycle and apoptosis. When specified control points of the cell cycle are detained, apoptotic cell death is triggered[42]. Accordingly, numerous anti-cancer drugs lead to cell cycle stoppage and clinically effective cancer treatment has been demonstrated [43]. This suggests that compound 6b has a stronger impact on HepG2 cells than compound 5. Compound 5 has an amino group bonded to a thaiadaiazoline ring, and free of the hydroxyl group. Whereas compound 6b has two aromatic rings bonded to a thaiadaiazoline ring and two hydroxyl groups. This range of functional groups boosts the compound's efficacy against liver cancer cells, paving the way for further research.

2.3. Molecular docking results

Molecular Bioinformatics Docking studies in the field of drug development are currently of considerable use, reducing the money and efforts required to screen novel compounds by directing and restricting the research to possible targets/targets. A molecular docking simulation is, thus, an essential way of anticipating a substrate interacting with its receptor.

To determine whether compounds 5 and 6b inhibits Akt1 and CDK4 proteins, thus, affecting cellular migration of HepG2, molecular docking simulation was carried out to determine the binding mode of 5 and 6b into the Akt1 and CDK4 active site. The 5 and 6b molecules were precisely docked into the active pocket of Akt1 and CDK4 in ADT software[44].

The results of the docking study showed a good fit into the binding of CDK4 protein active site with affinity energy -8.7 KJ/mol (6b) and -7.9 (5), the affinity energy of Akt1 protein with compound 6b (-10.0 KJ/mol). Moreover, the binding interactions between the amino acid residue and ligands (compounds 5 and 6b) are shown in Table 2 and Figures (5and 6). shown in figure 5 Compound 5 formed two hydrogen bonds, as a side-chain acceptor and backbone acceptor with amino acids (GLU A75 and LYS A180) residue of CDK4 protein. In addition, several hydrophobic interactions with amino acid residue include Lys A72, Gin B183, Glu A69, Lys B180and Thr B184. Compound 6b (figure 5) formed four hydrogen bonds as a side-chain acceptor with amino acid (GLU A69, Thr A184, GLU A69, and GLU A75) and ionic bond with GLU A69 of CDK4 protein, in addition, hydrophobic interactions with amino acid residue including Leu B188, Gin B261, Ser B258, Leu A65, and Cys A68. The interaction of compound 6b with Akt1 target protein (figure 6) shows two hydrogen bonds from binding with critical amino acid residues Trp A80, and Lys A268 as well as ionic interaction with Asp A292, Moreover, the hydrophobic interactions with amino acid residue including Tyr B205, Thr A82, Gin Arg B273, Val B270, Ser B205, Arg B273, and Leu B264. Compound 5 show one hydrogen bond with amino acid residue, Ile A 290, one ionic bond with Asp A 292, and one pi-pi interaction with Trp A 80 of Akt1 protein. In addition, several hydrophobic interactions with Leu B264, Leu B210, Ser B205, and Lys B268. The 3D molecular surface map of the most active compounds 5 and 6b docking into the HePG-2 binding site is shown in Figures 5and 6.

Table 2
Affinity Energy and amino acids residue of compounds 5 and 6b witha target protein.

Target protein	PDB ID	Compound	Binding interaction (Amino acid residue)	Interaction	Distance (A°)	Binding interaction Energy (Kcal/mol)	Affinity energy (Kcal/mol)
CDK4	2W96	6b	Glu 69 (A)	H-donor	2.85	-2.5	-10.1
			Thr 184 (A)	H-donor	3.44	-0.5	
			Glu 69 (A)	H-donor	2.94	-12.4	
			Glu 75 (A)	H-acceptor	3.59	-0.6	
			Glu 69 (A)	ionic	2.94	-4.9	
		5	Glu 75 (A)	H-donor	4.03	-1.4	-8.5
			Lys 180 (A)	H-donor	2.86	-2.2	
Akt1	5KCV	6b	Trp 80 (A)	H-acceptor	3.40	-0.6	-7.8
			Lys 268 (A)	H-acceptor	3.35	-1.3	
			Asp 292 (A)	ionic	3.80	-1.0	
		5	Ile 290 (A)	H-acceptor	2.95	-1.4	-7.6
			Asp 292 (A)	ionic	3.94	-0.6	
			Trp 80 (A)	pi-pi	3.89	0.0	

2.4. Molecular Dynamics simulation

Molecular dynamics is an analytical approach that uses computer simulation to analyze the physical motions of a predetermined amount of time is provided for the interaction of the atoms and molecules to reveal the system's complicated development. The design and discovery of novel medicines, it has shown to be a helpful tool. As a result of molecular dynamics research, thermodynamics and kinetics related to the compound–protein recognition and binding may be more precisely estimated. Root mean square deviation (RMSD), Root mean square fluctuation (RMSF), and Radius of gyration data as a function of time were used to analyze the molecular dynamic simulations[45]. In addition, Fig. (7) demonstrated that compound 6b-CDK4 complex has a higher ratio of water-binding with 17 amino acids for the active site of CDK4 as well as few hydrogen bonds. compound 5-CDK4 complex demonstrated a higher ratio of hydrogen bonds and water binding. As a result, compound 6b may have an active effect on CDK4, agreeing with the IC_{50} value.

Fig. (7C, D) showed the high ratio of hydrogen bond and water binding for Compound 5-AKT1, while compound 6-AKT1 showed hydrogen bonds and water binding.

RMSD and RMSF were used to analyze the molecular dynamic simulations, and assess internal motions conformation change and stability of compounds 5-CDK4, 6b-CDK4, 5-ART1, and 6b-ART1. The RMSD and RMSF values were shown in (Fig. 8, 9). In the compound 6b-CDK4 complex the scalar distance between atoms show an upward trend fluctuation from 0-25 nanosecond and the downward trend fluctuation from 25-100 nanosecond, the value of RMSD 1.7 Å, compound 5-CDK4 complex show an upward from 20-40, and 70-90 nanosecond, and downward from 40-70 nanosecond, the value of RMSD 1.6 Å. while compound 5-AKT1, and 6b-AKT1(Fig. 8C, D) showed the value conformation, that binding site less fluctuation. The RMSF values are used to predict the motion of compound- protein. The RMSF value of compound 5-CDK4 (Fig. 9A) demonstrated broad peaks 50-150Å with a value of (1.4-2.6)Å, compound 6b-CDK4 also showed broad peaks 90-200 ^{o}A with a value of (1.8-3.4)Å the RMSF of compound 5-ATK1 complex (Fig. 9C) it's related that sharp peaks (10-150)Å, had higher value (1.4-4) Å, compound 6b-CDK4 complex (Fig. 9D) showed sharp peaks (10-150) Å, with higher value (1.4-4.5) Å.

2.5. Bioinformatic results and discussion:

In the current study, we utilized UALCAN as a bioinformatics tool to highlight the expression of AKT1 and CDK4 in LIHC based on sample type (normal/primary tumor) and nodal metastasis status (N0: No regional lymph node metastasis; N1: Metastases in 1 to 3 axillary lymph nodes) using TCGA database. Substantially, our findings showed that AKT1 was expressed at much greater levels in primary tumors than in normal tissues(Figure 10A)and more abundant in N1 than in N0 and normal(Figure 10B). Similarly, CDK6 was highly expressed in primary tumors than in normal tissues(Figure 11A)and more considerable in N1 than in N0 and normal (Figure 11B). Our bioinformatic analysis showed that AKT1 and CDK4 are promising a druggable target to eradicate LIHC. As a consequence of the foregoing findings, it is indicated that the proposed compounds can combat LIHC and additional research on compound 6b is advised. We anticipate that the study will give ample references towards the development of a suitable scaffold for the LIHC.

2.6. Chemistry

The synthesis of two heterocyclic series of (thiazolidine-4-one and thiadiazole) derivatives are performed in multi-steps(Scheme 1 and 2), Initially, prepared thiosemicarbazone (1), then was treated with chloroacetic acid as a cyclized agent to prepare the first series from thaiazolidin-4-one[46]. The derivatives of thiazolidine-4-one (3a-e) were prepared by the reaction of a corresponding aromatic aldehyde with thiazolidine-4-one and sodium acetate as a reagent. the next series of thiadiazole was prepared from the reaction thiosemicarbazone with acetic anhydride[28], the product was treated with hydrazine monohydrate to hydrolysis the acetyl groups and prepare 2-amino thiadiazoline (5), the product was reacted with the corresponding aldehyde to form thiadiazole derivatives (6a and 6b).

2.7. Spectral characterization

The IR spectra of the synthesized compounds exhibits show bands of expected functional groups, the IR spectrum of thiosemicarbazone(47, 48), shows two bands at 3412 and 3346 cm^{-1} attributed to symmetric and asymmetric stretching of an amine group, strong band at 1087cm^{-1} attributed to stretching vibration of C=S, the thiosemicarbazone behavior has been reported in the literature (49-51).

Thiazolidine-4-one (2) shows a strong band within the range υ (1705-1770) cm^{-1} attributed to C=O, the absence of absorption bands of NH_2 and C=S group due to participate to form the thiazole ring with the synchronous appearance of new bands assigned to the carbonyl group within range υ (1705-1770) cm^{-1}. The IR spectrum of thaiadiazoline (4) shows two strong bands at 1707 and 1676 cm^{-1} attributed to C=O of acetyl groups also an absence of absorption bands of NH_2 and C=S group, with the synchronous appearance of new stretching vibration bands assigned to the carbonyl groups at 1707 and 1676 cm^{-1}, can be justified by a strain of thiadiazole ring and clearly displayed the involvement of the azomethine groups in the formation of five-membered rings. Thaiadiazoline's ring closure may be noted by the participation of azomethine (C=N) groups in nitrogen atom cyclization that is predicted to raise electron density in azomethines and to enhance the frequency of absorption (C=N) and the frequency of absorption is shifted about ($\upsilon \sim 30\ cm^{-1}$)(52).

The infrared spectrum of 5,5-diphenyl -1,3,4-thiadiazoline-2-amine (5) which formed by hydrolysis of thaiadiazoline displays two strong bands at υ (3421-3271)cm^{-1} attributed to the NH_2, also an absence of absorption bands of C=O of acetyl groups. Finally, the derivatives of thaiadiazolin show a strong band within range (1608-1631) cm^{-1} attributed to the azomethine group.

The data of ^1H NMR spectral of the synthesized compounds at room temperature in deuterated DMSO affirm the structure of compounds annotation and the formation of the heterocyclic ring in all compounds (53), thiosemicarbazone show the NH_2 signal at 8.41,8.37 ppm as two signals, also shown singlet signal at 8.64 ppm NH attributed to NH, the signals within range (7.34-7.67) ppm attributed to aromatic protons. The Thiazolidine-4-one (2) display signal at 11.9 NH and, singlet signal of $-CH_2-$ protons at 3.86 ppm. All protons in their predicted area are observed. Cyclic ring and $-CH_2-$ groups. Comparison of thiazolidine-4-one chemical shifts with thiosemicarbazide indicates that the NH2-proton signal in the spectrum is absent. The disappearance of NH2 proton signals from the ^1H NMR Thiazolidine-4-one spectrum supports cyclization of the thiosemicarbazone, which is confirmable by the appearance simultaneously of new signals of the five-membered ring. the spectra of (3a-3e) Thiazolidine-4-one derivatives display new signals with range (6.89-7.20) ppm attributed to C=CH of coupled groups with an absence of $-CH_2-$ protons of cyclic rings. Also, the spectra display signals of aromatic protons and protons signals of coupled groups. Thaiadiazolin (4) is produced from cyclization of the thiosemicarbazone. the spectrum shown two signals at 2.03 and 2.20 ppm attributed to OCH_3 also display signal at 11.73 ppm attributed to NH proton, all protons of cyclic, aromatic, and methyl can be seen In the predicted region, the Comparison of Thaiadiazolin (4) chemical shifts with thiosemicarbazide indicates that the NH_2 proton signal in the spectrum is absent. This confirms the formation of the

Thaiadiazolin ring. The spectra of compound 5 display a new signal at 6.23 ppm attributed to NH_2 protons with absent the signals of methyl protons, This supports the acetamide (HN-$COCH_3$) is hydrolysis and formed primary amine. The Thaiadiazolin derivative (6a-6b) spectra display the signal of azomethine within range (10.3-11.22) ppm and signals of phenolic protons within range (10.3-11.22) ppm as well as signals of aromatic protons.

The ^{13}C NMR spectra of synthesized compounds, the ^{13}C NMR spectrum of thiosemicarbazide (1) display signal at δ 178.3 ppm attributed to C=S carbon, also exhibits signal from C=N carbon at δ 149.5ppm. Furthermore, the ^{13}C NMR spectra give good evidence of cyclization of thiosemicarbazide through the absence of C=S from the thiazolidine-4-one spectrum, and a new signal appears at 33.2 ppm attributed to the C-S carbon signal from thiazolidine-4-one. Also, the spectrum of Thaiadiazolin (4) displays a signal at 85.6ppm attributed to C-S, it is from the cyclization of thiosemicarbazide through the absence of C=S from the spectrum. as well as the signals of C=O at 167.9, 170 ppm. the 6a and 6b spectra display azomethine (CH=N) carbon signal 164.6 ppm and 166.5 ppm respectively. All other carbon assignments were as anticipated(54). Mass spectrometry was used to determine the molecular ion peaks of synthesized compounds. The peak intensity provides information about the stability of fragments, especially with the base peak; the molecular ion confirms the proposed structural elucidation.

3. Conclusions

A new class of thiazolidine-4-one and thiadiazol derivatives have been designed and synthesized (1,2, 3a-3e, 4, 5, and 6a-6a). Using the DPPH method, we assessed the scavenger activity of compounds and discovered that compound 6b has the highest antioxidant activity, followed by compound 5. Furthermore, the cytotoxic activity of compounds 5 and 6b against HepG2 liver cancer cells revealed that compounds 5 and 6b are more toxic. Compound 5 arrested HepG2 cells in the S phase, while compound 6b resulted in a cellular arrest in the G1 phase, and both compounds decreased ROS and apoptosis. Docking studies with proteins Akt1 and CDK4 improved the results of compounds 5 and 6b. Docking studies revealed that both compounds make good contacts with protein binding sites. As a result, these two compounds should be developed as lead compounds for new liver cancer agents that inhibit Akt1 and CDK4.

4. Experimental Procedure

4.1 Instrumentation and spectral measurements

The IR spectra were collected by using FTIR-Affinity -1 spectrophotometer in the region 4000–400 cm^{-1} in KBr pellet. The mass spectra were scanned by the EI technique at 70 eV with an Agilent Technologies 5975C spectrometer. The experimental values of ^{1}H and ^{13}C NMR spectra for the studied compounds were scanned on a Bruker Avance 500 MHz spectrometer. TMS as the internal standard. DMSO-d6 was used as a solvent. Melting points were measured on an electrothermal apparatus. Elemental analysis (CHNS) was measured by using elementaryVario MICRO. UV-Visible were measured by

spectrophotometer type PG-instrument T80+. Microplate Reader Instrument using STAT FAX 2100, BioTek, Winooski, USA.

4.2. Chemistry section

Two types of heterocyclic derivatives were prepared from thiosemicarbazone. The first type is thiazolidine-4-one and its derivatives, the second type is thaiadaiazoline derivatives.

4.2.1. Procedure for synthesis 2-(diphenyl methylene)hydrazine-1-carbothioamide (1):

Thiosemocarbazide (0.914g, 10 m.mol) was added to hot ethanol and (1.822g, 10m.mol) of benzophenone with 1ml of glacial acetic acid, the reaction mixture was refluxed for 3h Then cool down to room temperature, the solid product was filtered, dried and finally recrystallization from ethanol.

White crystals, yield: 90%, M.p: 173–172°C.^{1}H NMR (DMSO, δppm):7.34 (t,3H,*J*= 5Hz, Ar-H)7.38(t,3H,*J*=5Hz,Ar-H)7.64(d,2H,*J*=5Hz,Ar-H)7.67 (d,2H,*J*=5Hz,Ar-H)8.41- 8.37 (s, 2H, NH_2)8.64(s, H,NH).^{13}C NMR (DMSO, δppm) 128 ,130,131,136.7, 149.5, 178.3..IR (υ, cm^{-1}):3412, 3346, 3250,3053,1496,1481, 3053, 1325, 650.MS (70 eV, m/z) : 255.34[M], 238, 222.2, 195.2, 180.1, 165.1, 77.1. Anal. calc. for:$C_{14}H_{13}N_3S$:C, 68.65; H, 5.83; N, 17.46; S, 13.26, found: C, 66.96; H, 5.33; N, 16.92; S, 12.87.

4.2.2.Procedure for synthesis 2-((diphenylmethylene)hydrazineylidene)thiazolidin-4-one (2):

Compound 2 was prepared from thiosemicarbazone (1) with cyclization agent chloroacetic acid and sodium acetate. The thiosemicarbazone(1) (1.2g, 4 m.mol) was dissolved in 50ml ethanol and added chloroacetic acid (0.8g, 4m.mol), sodium acetate (1.32g, 16m.mol), the reaction mixture was refluxed for 8hrs, after the reaction completion cools down to room temperature, then it was poured to cool water, it was kept overnight, the reaction mixture filtered and recrystallization from ethanol.

Pale yellow crystals, yield: 73%, M.p: 185–186°C.^{1}H NMR (DMSO, δ ppm): 3.86 (S,2H), 7.23(t,3H, *J*=5Hz,Ar-H), 7.42(t,3H, *J*=5Hz, Ar-H), 7.45(d,2H,*J*=5Hz,Ar-H), 7.53(d,2H,*J*=5Hz,Ar-H), 11.90(s ,H, NH). ^{13}C NMR (DMSO, δ ppm): 33.2, 128.3-138.1,162.1, 174.3, C=O: 226.8. IR (υ, cm^{-1}): 3124,3062, 2962, 1705, 1616,1585, 1490, 1442, 1317,1165, 696. MS (70 eV, m/z):295.36 [M], 248.2, 218.2, 207.1, 195.2, 180.1, 165, 115, 77.2. Anal. calc. for:$C_{16}H_{13}N_3OS$,C, 65.07; H, 4.44; N, 14.23; S, 10.85, found: C, 64.56; H, 4.13; N; 13. 93; S, 10.16.138.1,162.1, 174.3, C=O: 226.8. IR (υ, cm^{-1}): 3124,3062, 2962, 1705, 1616,1585, 1490, 1442, 1317,1165, 696. MS (70 eV, m/z):295.36 [M], 248.2, 218.2, 207.1, 195.2, 180.1, 165, 115, 77.2. Anal. calc. for:$C_{16}H_{13}N_3OS$,C, 65.07; H, 4.44; N, 14.23; S, 10.85, found: C, 64.56; H, 4.13; N; 13. 93; S, 10.16.

4.2.3.General Procedure for synthesis thiazolidine -4-one derivatives (3a-3e)

An equimolar amount of thiazolidine-4-one (2) and the corresponding aldehyde (0.2 m.mol)

Dissolved in glacial acetic acid (20ml), then added anhydrous sodium acetate (1.2g) the was heated at 120^{o}C in an oil bath, the reaction mixture was monitored by TLC using (chloroform: ethanol) (8:2 v/v), after cool down to room temperature, the mixture reaction was poured to (100ml) ice water and kept it overnight, the solid product was filtered, recrystallization from an appropriate solvent.

4.2.3.1.: 5-((Z)-4-hydroxybenzylidene)-2-((diphenylmethylene) hydrazineylidene)-thiazolidin-4-one (3a):

Orange crystals, recrystallized from ethanol, yield: 62%, M.p: 162–164°C.^{1}H NMR (DMSO, δ ppm): 6.97(s,1H ,Ar-H), 7.24-7.53(m,14H, Ar-H), 8.09(s, 1H,OH), 11.92(s, 1H, NH).^{13}C NMR (DMSO, δ ppm): 128.3-134.7,162.1, 163.4, 165.7, 194.4; IR (υ, cm^{-1}) : 3414, 3150, 3062, 2920, 2920,1705, 1612, 1585, 1492, 1442, 1317. MS (70 eV, m/z): 399.47 [M], 322.1, 294.1, 195.2, 180.1, 165, 77.1. Anal. calc. for: $C_{23}H_{17}N_3O_2S$,C, 69.16 ; H, 4.29; N, 10.52; S, 8.03, found: C, 67.34; H, 4.11; N, 10.07; S, 8.56.

4.2.3.2.: 5-((Z)-2,4-dihydroxybenzylidene)-2((diphenylmethylene) hydrazineylidene) thiazolidin-4-one (3b):

Pale yellow crystals, recrystallized from ethanol, yield: =60%, M.p: 165–166°C.^{1}H NMR (DMSO, δ ppm): 7.11(s,1H, Ar-H), 7.12(s,H,Ar-H), 7.24(d, H, *J*=5Hz, Ar-H),7.42 (d, H, *J*=10Hz,Ar-H)7.45 (t,6H, *J*=5Hz,Ar-H), 7.53 (d, 2H,*J*= 10Hz,Ar-H), 7.57 (d, 2H, *J*=10Hz ,Ar-H), 10.13(s, OH),11.08 (s,OH), 11.90(s ,H, NH).^{13}C NMR (DMSO, δ ppm): 122.3-136.2, 137.2, 154.7, 161.6, 162.7, 164, 166.5, 187.7. IR (υ, cm^{-1}):3431, 3143, 3062, 2937,1705, 1612, 1585, 1490, 1444, 1317, 696. MS (70 eV, m/z): 415.47[M],398.1, 294.1,222.2, 180.1, 165.2 77.2. Anal. calc. for:$C_{23}H_{17}N_3O_3S$,C, 66.49; H, 4.12; N, 10.11; S, 7.72, found: C, 65.61; H, 3.93; N, 9.66; S, 7.14.

4.2.3.3.: 5-((Z)-3,4-dihydroxybenzylidene)-2((diphenylmethylene) hydrazineylidene) thiazolidin-4-one (3c):

Pale yellow crystals, recrystallized from methanol, yield: =69%, M.p: 157–159°C.^{1}H NMR (DMSO, δ ppm):): 7.09(s,1H, Ar-H), 7.12(s,H,Ar-H), 7.24(d, H,*J*=5Hz, Ar-H), 7.36 (d, H, *J*=10Hz,Ar-H), 7.42 (t,3H, *J*=5Hz,Ar-H), 7.47 (t,3H,*J*= 10Hz,Ar-H), 7.53 (d,2H, *J*=10Hz,Ar-H), 7.79 (d,2H,*J*=10Hz,Ar-H), 10.21(s,1H,OH), 11.08(s,1H, OH), 11.90(s ,1H, NH). ^{13}C NMR (DMSO, δ ppm): 128.3-138.1, 147.7, 156.6, 162.1, 165.9, 172, 174.3, 186. IR (υ, cm^{-1}): 3441, 3123, 3064,2937, 1705, 1622, 1585, 1492, 1429, 696. MS (70 eV, m/z): 415.47[M], 398.1, 338, 294.1, 222.1, 195.2, 165, 77.2. Anal. calc. for: $C_{23}H_{17}N_3O_3S$,C, 66.49; H, 4.12; N, 10.11; S, 7.72, found: C, 65.83; H, 3.83; N, 9.96; S,7.25.

4.2.3.4:5-((Z)-4-(methylthio)benzylidene)-2-((diphenylmethylene)hydrazineylidene) thiazolidin-4-one (3d):

Pale yellow crystals, recrystallized from ethylacetate, yield: =51%, M.p: 169–170°C.^{1}H NMR (DMSO, δ ppm): 2.54(s,3H,SCH_3), 7.22(s ,s,1H,olefinic protons), 7.26 (d,2H, *J*=10Hz,Ar-H), 7.32 (d,2H,*J*=10Hz,Ar-H), 7.41(t,3 H,*J*=5Hz,Ar-H), 7.44(t,3 H,*J* = 10Hz ,Ar-H), 7.49(d,2 H,*J*=5Hz,Ar-H), 7.58(d ,2H,*J*=10Hz,Ar-H). ^{13}C NMR (DMSO, δ ppm): 16.7, 128.3-133.8, 136.7 ,136.7, 139.8, 149.5, 161.4, 178, IR (υ, cm^{-1}): 3431, 3078,2920, 1705, 1612, 1583, 1492, 1444, 1317, 1165, 696.MS (70 eV, m/z):429.56 [M], 294.2, 195.2,

180.1, 165, 149.2, 77, 43. Anal. calc. for$C_{24}H_{19}N_3OS_2$:C, 67.11; H, 4.46; N, 9.78; S, 14.93, found: C, 66.15; H, 4.19; N, 9.06; S, 14.42.

4.2.3.5: (5Z)-5-(benzo[d][1, 3]**dioxol-5ylmethylene)-2 ((diphenylmethylene) hydrazineylidene) thiazolidin-4-one (3e)** :

Pale yellow crystals, recrystallized from ethylacetate, yield: =81%, M.p: 174–176°C.^{1}H NMR (DMSO, δ ppm): 6.06(s,2H,CH_2), 6.89(s, 1H, Ar-H), 6.95(s, H, ,Ar-H), 7.11 (d, *J*=15Hz,Ar-H), 7.24 (d, *J*=10Hz,Ar-H), 7.41(t,3 H,*J*=5Hz,Ar-H), 7.48(t,2 H,*J*= 10Hz,Ar-H), 7.52(d,2 H,*J*=5Hz,Ar-H), 11.90(s ,H, NH). ^{13}C NMR (DMSO, δ ppm) : 102, 120.2-134.7, 136.2 ,138.1,162.1,166, 171.8, 174.3, 186.6. IR (υ, cm^{-1}): 3442, 3078,2818, 1705, 1610, 1583, 1490, 1444, 1344, 1041, 696. MS (70 eV, m/z):427.48 [M], 294.2, 248.2, 195.1, 180.1, 165, 121.4, 77.2. Anal. calc. for: $C_{24}H_{17}N_3O_3S$,C, 67.43; H, 4.01; N, 9.81; S, 7.50, found: C, 66.27; H, 3.82; N, 10.26; S, 7.12.

4.2.4: Procedure for synthesis N-(4-acetyl-5,5-diphenyl-4,5-dihydro-1,3,4-thiadiazol-2-yl) acetamide (4):

Thiosemicarbazone (1) (1.82g, 7.156m.mol) was dissolved in 40 ml acetic anhydride, the reaction mixture was heated in an oil bath at 118-120^{o}C at 20 hrs, the progress of the reaction mixture was monitored by TLC using (benzene: ethyl acetate), (6:4 v/v), the reaction mixture was cool down to room temperature and poured to 200 ml ice water, then was kept it at room temperature, then the filtered it, was recrystallization from ethanol.

White crystals, yield: 61%, M.p: 195–196°C.^{1}H NMR (DMSO, δ ppm): 2.03(s,3H ,$COCH_3$), 2.20(s,3H ,$COCH_3$), 7.32 (d,4H, *J*=10Hz,Ar-H), 7.38(t,6H, ,*J*=5Hz,Ar-H), 11.73(s ,H, NH). ^{13}C NMR (DMSO, δ ppm):22.8, 24.2, 85.6, 128.1-128.4,140.8, 148, 167, C=O: 170. IR (υ, cm^{-1}): 3450, 3059,2935, 1707, 1676, 1597, 1492, 1442, 1328, 1180, 698.MS (70 eV, m/z):339.41 [M],297.2, 281, 238.1, 195.2, 180.1, 165.2, 77.2, 43.3. Anal. calc. for: $C_{18}H_{17}N_3O_2S$,C, 63.70; H, 5.05; N, 12.38; S, 9.45, found: C, 62.95; H, 4.87; N, 11.66; S, 882.

4.2.5: Procedure for synthesis5,5-diphenyl -1,3,4-thiadiazoline-2-amine(5):

Compound (4) (0.678g, 8 m.mol) was dissolved in 10 ml of ethanol, hydrazine mono hydrate (6.8 ml) was added to the reaction mixture drop wise with stirring, slowly raising the temperature to the reflux for 3hrs. the progress of the reaction was monitored by TLC using (ethanol; chloroform) (2:8 v/v), after completion the reaction, the reaction mixture was cool down to room temperature, then it was filtered and recrystallized from ethanol. yellow crystals, yield: 62%, M.p: 90–91°C.^{1}H NMR (DMSO, δ ppm): 6.23(s ,2H, NH_2), 7.23(t,2H,*J*=10Hz,Ar-H), 7.28(t,2H, *J*=10Hz,Ar-H), 7.33(d,2H, ,J=10Hz,Ar-H), 7.49(d,2H, ,J=5Hz,Ar-H), 7.56(t,2H, *J*=5Hz,Ar-H), ^{13}C NMR (DMSO, δ ppm): 25.9, 127.6-129.8, 129.8, IR (υ, cm^{-1}): 3421, 3271,3080,1610, 1492, 1442, 1336, 1180, 696.MS (70 eV, m/z): 255.34 [M],195.3, 180.1, 165.2, 77.2. Anal. calc. for:$C_{14}H_{13}N_3S$, C, 65.86; H, 5.13; N, 15.46; S, 12.56, found: C, 64.80; H, 4.92; N, 15.16; S, 11.89.

4.2.6: General Procedure for synthesis 1,3,4-thiadiazoline derivatives (6a, 6b)

5,5-diphenyl -1,3,4-thiadiazoline-2-amine (5) (0.635g, 2.5 m.mol) was dissolved in 40 ml ethanol, corresponding aldehyde (2.5 m.mol) and 0.5 ml glacial acetic acid was added to the reaction mixture, the mixture was refluxed 5hrs, forming of the products was confirmed TLC using (ethanol; ethyl acetate) (1:9 v/v), after completion the reaction was it cool down to room temperature, then it was filtered and recrystallization from an appropriate solvent.

4.2. 6.1: (Z)-4-(((5,5-diphenyl -1,3,4-thiadiazoline-2-yl) imino)methyl)phenol(6a):

yellow crystals, recrystallized from ethanol, yield: 60%, M.p: 175-177°C.^{1}H NMR (DMSO, δ ppm): 6.79(s,H,NH), 6.80-7.61(m,14 H, *J*=10Hz, Ar-H),8.49 (s,H, CH=N), 10.03(s,1H,OH). ^{13}C NMR (DMSO, δ ppm): 116, 128.1-138.2, 159.5, 160.7, 164.6. IR (υ, cm^{-1}): 3342, 3124,3055 ,1608, 1585,1516, 1492, 1305, 694. MS (70 eV, m/z): 359.45[M], 283.2, 239.1, 195.1, 165.1, 77.2. Anal. calc. for: $C_{21}H_{17}N_3OS$, C, 70.17; H, 4.77; N, 11.69; S, 8.92, found: C, 69.21; H, 4.13; N, 11.06; S, 8.02.

4.2.6.2: **(Z)-4-(((5,5-diphenyl -1,3,4-thiadiazoline-2-yl) imino)methyl) benzene-1,3-diol (6b)**

yellow crystals, recrystallized from methanol, yield: 75%, M.p: 168-169°C.,^{1}H NMR (DMSO, δ ppm): 6.35(s ,1H,NH),6.37(s ,H, Ar-H), 7.28(d,1H, *J*=10Hz,Ar-H), 7.36 (d,H, ,*J*=10Hz,Ar-H)7.45(t,3H, ,*J*=5Hz,Ar-H), 7.52(t,3H ,*J*=10Hz,Ar-H), 7.65 (d,4H, *J*=10 Hz ,Ar-H), 8.81(s, H, CH=N), 10.20(s,H_{26},OH), 11.22(s,H_{27},OH), ^{13}C NMR (DMSO, δ ppm): 102.7, 108.5, 110.7,128.6-137.2, 161.6, 164.1, 166.5. IR (υ, cm^{-1}): 3317, 3142,3055 ,1631, 1606, 1506, 1489, 1323, 692.MS (70 eV, m/z): 375.45 [M] ,316.2, 299.1, 239.1, 180.1, 165.1, 77.2. Anal. calc. for:$C_{21}H_{17}N_3O_2S$, C, 67.18; H, 4.56; N, 11.19; S, 8.54, found: C, 66.55; H, 5.26; N, 10.56;S, 7.82.

5. Dpph Radical Scavenging Assay

The antioxidant activity of all the synthesized compounds was an evaluation by determining the ability of radical scavenging according to the Blois method [55]. The inhibitory activity of DPPH was measured by using the spectrophotometer method by mixing 1ml of different concentrations (50, 75, 100, and 200) μM of solution of synthesized compounds with 1ml of 200 μM of DPPH solution, the absorbance was measured at 517nm after 70min. The inhibition percentage calculates by using the following equation:

$$\text{inhibition percentage } \% = \frac{Ac - As}{As} \times 100$$

Ac = control absorbance, the absorbance of DPPH without sample

As = sample absorbance, the absorbance of DPPH with sample

6. Mtt Assay

The cell line was mainly grown in 96-well plates at 1x105 cells per well for 24 hours under optimum conditions (37°C, 5% CO2 in a humidified incubator). Next, the cells were washed twice with PBS after the removal of the growth medium (10% FBS). New culture media containing the studied compounds at a concentration (5, 10, 25, 25) µM were added to the cells followed by incubation for24, 48, and 72 h. Quintet wells were analyzed for each concentration. A 10µL solution of freshly prepared (5 mg/mL) MTT in PBS was added to each well and then incubated for an additional 4 hours. After successful incubation, the resulting medium was aspirated and the MTT formazan which has been generated in this step was dissolved in the 100 µL of DMSO. The solubilization of formazan crystals was obtained by gently shaking the plates. A microplate reader was then employed to measure the absorbance at 545 nm. The cellular toxicity percentage, as well as the half-maximal inhibitory concentration (IC_{50}), were calculated by the following equation [56, 57].

$$\text{Viability } \% = \frac{\text{mean of OD sample}}{\text{mean of OD control}} \times 100$$

7. Flow Cytometry Analysis

7.1. Cell Cycle

According to Al-Shawi et al. [58], flow cytometry analysis identified the G1, S, and G2 phases for compounds 5 and 6b. a system with some modifications. The IC_{50} values of compounds 5 and 6b were added to HepG2 cells for 48 hours. The cells were washed in PBS followed by fixation in 70% ice-cold ethanol overnight at 4°C. After being washed twice with PBS, cells were then stained with a solution containing 50 g/ml PI and 100 g/ml RNase A for 30 minutes in the dark at room temperature. Flow cytometry was employed to investigate the labeled cells (Beckman Coulter, Epics XL).

7.2. Reactive oxygen species

The cells were stained with 2,7-dichlorofluorescein-diacetate to determine the changes within the intracellular reactive oxygen species generation, as described by Khan et al. with some modifications [59]. (DCFH-DA) Formalized adverbial in a nutshell, HepG2 cells were cultured in 6 well culture plates overnight. The cells were examined 48 hours after treatment with or without the IC_{50} value of compounds 5 and 6b. The cells were then incubated for 30 minutes at 37°C with 10 mol/l DCFH-DA, per the manufacturer's instructions. The cells were then incubated for 30 minutes at 37°C with 10 mol/l DCFH-DA, as directed by the manufacturer. In the positive control group, DCFH-DA labeled cells were treated with 1 l rose for 30 minutes. The cells were then harvested, rinsed, resuspended in PBS, filtered through 300 apertures, and flow cytometry was used to search for DCF fluorescence (FCM).

7.3. Apoptosis

Flow cytometry analysis, which was adapted from the Wang et al. method[60], was used to identify early and late apoptosis. Compounds 5 and 6b IC_{50} values were applied to HepG2 cells for 48 hours. The cells

were collected, rinsed twice with PBS, and labeled with 5 ul FITC-conjugated annexin V, as directed by the manufacturer. After being incubated in the dark for 10 minutes and then labeled with PI. Samples were then analyzed on a flow cytometer (Beckman Coulter, Epics XL).

8. Molecular Docking

As usual, the receptor input files were created. To begin, we removed any water molecules, ligand atoms, and ions that did not belong to the receptor's active site from the PDB file. After that, hydrogen atoms, protons, and partial charges from amino acid side chains were added (following the protonation state at the physiological). This was followed by a local minimization to relieve potential bad contacts. Minimization was performed in the presence of restraints to maintain the protein conformation. The structure of ligands (compound 5 and 6b) was drawn using Chem Draw Ultra from the Chem Office software package. Then, it was copied into Chem3D Ultra (same program package), before using ADT, it's a good idea to check that the file contains all hydrogen atoms. ADT now immediately computes Gasteiger charges (empirical atomic partial charges) and distinguishes between hybridization states and atom groups after opening the ligand. The software specifies the ligand's rotatable bonds as part of the preparation process so that different conformers for docking can be produced. Where it was subjected to a simplified energy minimization search to a minimum root mean standard deviation gradient of 0.100. The obtained structure with local minimum was saved in convenient mol2 format.

Docking studies [61].was confuted using Auto Dock vena to obtain binding interaction between the ligand (compound 5 and 6b) and binding pockets of two distinct proteins of liver cancer cell (HepG-2). From the protein data bank (https://www.rcsb.org/). The crystal structure of Hepg-2 proteins was obtained: Akt1 (PDB: ID 5KCV) [62], and CDK4 (DPB: ID 2W96) [63]. Energy minimization and hydrogen bonding optimization were carried out after docking. For each ligand the docking simulation was run multiple times for further study, the highest binding scores were used in addition. Discovery studio visualizes 2019 was used to do a thorough examination of the docking effects.

9. Statistical Analysis

IC_{50} values of the compounds were performed by plotting dose-response curves vs. the concentrations using GraphPad Prism version 8.1 for windows. The experiment was repeated thrice.

10. Bioinformatic Analysis

To highlight many discoveries linked to our targets AKT1and CDK4, we used a variety of bioinformatics approaches. First, UALCAN is a web-based resource for cancer research that is comprehensive, user-friendly, and interactive. UALCAN is meant to give users quick access to publically available TCGA data, allowing them to find biomarkers and perform in silico validation of possible genes of interest, as well as display expression profiles and patient survival statistics in graphs and plots for various cancer types [64].

Second, TIMER is a comprehensive resource for studying immune infiltrates in malignancies of diverse types methodically. We used the latest version of the website to estimate the amount of immune infiltrates using multiple immune deconvolution algorithms, produce high-quality figures dynamically, and examine tumor immunological, clinical, and genetic features in-depth in the current study [5].

We utilized TIMER as a bioinformatic tool to show the Kaplan-Meier curves for the associated immune infiltrates (CD8+ T cells, CD4+ T cells, Tregs, B cells, Neutrophil, Monocytes, Macrophages M0, Macrophages M1, Macrophages M2, Dendritic cells (DC), Nature Killer cells (NK), Mast cells, Endothelial cells, Hematopoietic stem cells, Eosinophils, Common lymphoid progenitor, Common myeloid progenitor, Cancer associated fibroblasts, T cell Follicular Helper, T cell gamma delta and T cell NK) in Liver Hepatocellular Carcinoma (LIHC). In a multivariable Cox proportional hazard model, the outcome module allows us to explore the clinical relevance of tumor immune subsets while enabling us to account for various factors. The hazard ratio, p-value for the Cox model for the Kaplan-Meier curves are separated into low and high levels of infiltration. Furthermore, the gene module displays a scatter plot and the purity-adjusted spearman's rho to visualize the association of AKT1 and CDK4 expression with immune infiltration level in LIHC. Because most immune cell types are negatively related to tumor purity, tumor purity is a significant confounding factor in our investigation[65].

We also used the gene outcome modules to generate Kaplan-Meier curves to show the clinical significance of AKT1 and CDK4 expression in LIHC patients. We utilized the Cox proportional hazard model to assess the outcome significance of gene expression in this study[66].

Third, Cycle base 3.0 is a web-based database that incorporates new mRNA and protein expression data, as well as cell-cycle phenotypic information from high-content screens and model-organism databases used in genome-wide cell-cycle research [67]. We evaluated the role of AKT1 and CDK4 expression during distinct stages of the cell cycle in the current proposal.

References

1. Cronin KA, Lake AJ, Scott S, Sherman RL, Noone AM, Howlader N, et al. Annual Report to the Nation on the Status of Cancer, part I: National cancer statistics. Cancer. 2018;124(13):2785-800.

2. Xia Z-K, Wang W, Qiu J-G, Shi X-N, Li H-J, Chen R, et al. Discovery of a New CDK4/6 and PI3K/AKT Multiple Kinase Inhibitor Aminoquinol for the Treatment of Hepatocellular Carcinoma. Frontiers in pharmacology. 2021;12.

3. Zhao J-X, Yuan Y-W, Cai C-F, Shen D-Y, Chen M-L, Ye F, et al. Aldose reductase interacts with AKT1 to augment hepatic AKT/mTOR signaling and promote hepatocarcinogenesis. Oncotarget. 2017;8(40):66987.

4. Lu J-W, Lin Y-M, Chang J-G, Yeh K-T, Chen R-M, Tsai JJ, et al. Clinical implications of deregulated CDK4 and Cyclin D1 expression in patients with human hepatocellular carcinoma. Medical oncology.

2013;30(1):379.

5. El-Arabey AA, Abdalla M, Abd-Allah AR. SnapShot: TP53 status and macrophages infiltration in TCGA-analyzed tumors. International Immunopharmacology. 2020;86:106758.

6. Xiao S, Wang X, Xu L, Li T, Cao J, Zhao Y. Novel panaxadiol triazole derivatives induce apoptosis in HepG-2 cells through the mitochondrial pathway. Bioorganic Chemistry. 2020;102:104078.

7. Zhang J, Wang X, Yang J, Guo L, Wang X, Song B, et al. Novel diosgenin derivatives containing 1, 3, 4-oxadiazole/thiadiazole moieties as potential antitumor agents: Design, synthesis and cytotoxic evaluation. European journal of medicinal chemistry. 2020;186:111897.

8. Belluco P, Gaion R, Maragno I, Dorigo P. Etozoline and vascular spasm. Pharmacological research. 1990;22:123-4.

9. Eissa IH, Dahab MA, Ibrahim MK, Alsaif NA, Alanazi A, Eissa SI, et al. Design and discovery of new antiproliferative 1, 2, 4-triazin-3 (2H)-ones as tubulin polymerization inhibitors targeting colchicine binding site. Bioorganic Chemistry. 2021;112:104965.

10. Lu H, Zhang H, Jiang Y. Methazolamide in high-altitude illnesses. European Journal of Pharmaceutical Sciences. 2020;148:105326.

11. Abo-Bakr AM, Hashem HE. New 1, 3, 4-thiadiazole derivatives: synthesis, characterization, and antimicrobial activity. Journal of Heterocyclic Chemistry. 2019;56(3):1038-47.

12. Alho M, Moglioni A, Brousse B, Moltrasio G, D'Accorso N. Synthesis and characterization of 2, 2-disubstituted thiadiazolines. Arkivoc. 2000;2000(4 SPECISS):627-40.

13. Wu Q, Cai H, Yuan T, Li S, Gan X, Song B. Novel vanillin derivatives containing a 1, 3, 4-thiadiazole moiety as potential antibacterial agents. Bioorganic & medicinal chemistry letters. 2020;30(10):127113.

14. Abdelhameid MK, Zaki I, Mohammed MR, Mohamed KO. Design, synthesis, and cytotoxic screening of novel azole derivatives on hepatocellular carcinoma (HepG2 Cells). Bioorganic chemistry. 2020;101:103995.

15. Appalanaidu K, Kotcherlakota R, Dadmal T, Bollu VS, Kumbhare RM, Patra CR. Synthesis and biological evaluation of novel 2-imino-4-thiazolidinone derivatives as potent anti-cancer agents. Bioorganic & medicinal chemistry letters. 2016;26(21):5361-8.

16. Carvalho SA, da Silva EF, Santa-Rita RM, de Castro SL, Fraga CA. Synthesis and antitrypanosomal profile of new functionalized 1, 3, 4-thiadiazole-2-arylhydrazone derivatives, designed as non-mutagenic megazol analogues. Bioorganic & medicinal chemistry letters. 2004;14(24):5967-70.

17. Mohamed AH, Ramadan M. Synthesis and colon anticancer activity of some novel thiazole/-2-quinolone derivatives. Journal of Molecular Structure. 2020;1207:127798.

18. Prabhakar YS, Solomon VR, Gupta MK, Katti S. QSAR studies on thiazolidines: a biologically privileged scaffold. QSAR and Molecular Modeling Studies in Heterocyclic Drugs II: Springer; 2006. p. 161-249.

19. Prashantha Kumar B, Basu P, Adhikary L, Nanjan M. Efficient conversion of N-terminal of L-tyrosine, DL-phenyl alanine, and glycine to substituted 2-thioxo-thiazolidine-4-ones: a stereospecific synthesis. Synthetic Communications. 2012;42(20):3089-96.

20. Tahlan S, Kumar S, Ramasamy K, Lim SM, Shah SAA, Mani V, et al. In-silico molecular design of heterocyclic benzimidazole scaffolds as prospective anticancer agents. BMC chemistry. 2019;13(1):1-22.

21. Weis S, Kesselmeier M, Davis J, Morris A, Lee S, Scherag A, et al. Cefazolin versus anti-staphylococcal penicillins for the treatment of patients with Staphylococcus aureus bacteraemia. Clinical Microbiology and Infection. 2019;25(7):818-27.

22. Almandil NB, Taha M, Rahim F, Wadood A, Imran S, Alqahtani MA, et al. Synthesis of novel quinoline-based thiadiazole, evaluation of their antileishmanial potential and molecular docking studies. Bioorganic chemistry. 2019;85:109-16.

23. Pushkarevsky NA, Lonchakov AV, Semenov NA, Lork E, Buravov LI, Konstantinova LS, et al. First charge-transfer complexes between tetrathiafulvalene and 1, 2, 5-chalcogenadiazole derivatives: Design, synthesis, crystal structures, electronic and electrical properties. Synthetic Metals. 2012;162(24):2267-76.

24. Semenov NA, Pushkarevsky NA, Suturina EA, Chulanova EA, Kuratieva NV, Bogomyakov AS, et al. Bis (toluene) chromium (I)[1, 2, 5] thiadiazolo [3, 4-c][1, 2, 5] thiadiazolidyl and [1, 2, 5] thiadiazolo [3, 4-b] pyrazinidyl: New heterospin (S 1= S 2= 1/2) radical-ion salts. Inorganic chemistry. 2013;52(11):6654-63.

25. Ebrahimi HP, Hadi JS, Alsalim TA, Ghali TS, Bolandnazar Z. A novel series of thiosemicarbazone drugs: from synthesis to structure. Spectrochimica Acta Part A: Molecular and Biomolecular Spectroscopy. 2015;137:1067-77.

26. Janowska S, Paneth A, Wujec M. Cytotoxic Properties of 1, 3, 4-Thiadiazole Derivatives—A Review. Molecules. 2020;25(18):4309.

27. Kakekochi V, Chandrasekharan K, Kumar U. Impact of donor–acceptor alternation on optical power limiting behavior of H–Shaped thiophene–imidazo [2, 1-b][1, 3, 4] thiadiazole flanked conjugated oligomers. Dyes and Pigments. 2020;175:108181.

28. Saiz C, Pizzo C, Manta E, Wipf P, Mahler SG. Microwave-assisted tandem reactions for the synthesis of 2-hydrazolyl-4-thiazolidinones. Tetrahedron letters. 2009;50(8):901-4.

29. Trotsko N, Bekier A, Paneth A, Wujec M, Dzitko K. Synthesis and in vitro anti-Toxoplasma gondii activity of novel thiazolidin-4-one derivatives. Molecules. 2019;24(17):3029.

30. Bade TS, Ebrahimi HP, Alsalim TA, Titinchi SJ, Abbo HS, Bolandnazar Z, et al. A novel series of 1, 4-Dihydropyridine (DHP) derivatives bearing thiazolidin-4-one: From synthesis to structure. Journal of Molecular Structure. 2017;1138:136-48.

31. Feitoza DD, Alves AJ, Lima JGd, Araújo JM, Aguiar JS, Rodrigues MdD, et al. Synthesis, antimicrobial and cytotoxic activities of 5-benzylidene-2-[(pyridine-4-ylmethylene) hydrazono]-thiazolidin-4-one and 2-[(pyridine-4-ylmethylene) hydrazono]-thiazolidin-4-one derivatives. Química Nova. 2012;35:694-8.

32. Gomha SM, Khalil KD. A convenient ultrasound-promoted synthesis of some new thiazole derivatives bearing a coumarin nucleus and their cytotoxic activity. Molecules. 2012;17(8):9335-47.

33. Девіняк ОТ, Гаврилюк ДЯ, Авдєєв СС, Чумак ВВ, Панчук РР, Стойка РС, et al. Virtual screening and its experimental validation reveal novel compounds with promising anticancer activity among 4-thiazolidinone-pyrazoline-and isatin-based conjugates. 2014.

34. Pong K. Oxidative stress in neurodegenerative diseases: therapeutic implications for superoxide dismutase mimetics. Expert opinion on biological therapy. 2003;3(1):127-39.

35. Duru R, Njoku O, Maduka I. Oxidative stress indicators in patients with prostate disorders in Enugu, South-East Nigeria. BioMed research international. 2014;2014.

36. Jothy SL, Zuraini Z, Sasidharan S. Phytochemicals screening, DPPH free radical scavenging and xanthine oxidase inhibitiory activities of Cassia fistula seeds extract. Journal of Medicinal Plants Research. 2011;5(10):1941-7.

37. Slavova-Kazakova AK, Angelova SE, Veprintsev TL, Denev P, Fabbri D, Dettori MA, et al. Antioxidant potential of curcumin-related compounds studied by chemiluminescence kinetics, chain-breaking efficiencies, scavenging activity (ORAC) and DFT calculations. Beilstein journal of organic chemistry. 2015;11(1):1398-411.

38. Ferlay J, Soerjomataram I, Dikshit R, Eser S, Mathers C, Rebelo M, et al. Cancer incidence and mortality worldwide: sources, methods and major patterns in GLOBOCAN 2012. International journal of cancer. 2015;136(5):E359-E86.

39. Zhang Q, Bao J, Yang J. Genistein-triggered anticancer activity against liver cancer cell line HepG2 involves ROS generation, mitochondrial apoptosis, G2/M cell cycle arrest and inhibition of cell migration. Archives of medical science: AMS. 2019;15(4):1001.

40. Muğlu H, Yakan H, Shouaib HA. New 1, 3, 4-thiadiazoles based on thiophene-2-carboxylic acid: Synthesis, characterization, and antimicrobial activities. Journal of Molecular Structure.

2020;1203:127470.

41. Szeliga M. Thiadiazole derivatives as anticancer agents. Pharmacological Reports. 2020:1-22.

42. Pathak N, Khandelwal S. Role of oxidative stress and apoptosis in cadmium induced thymic atrophy and splenomegaly in mice. Toxicology letters. 2007;169(2):95-108.

43. Xiao-Ming Y. Signal transduction mediated by Bid, a pro-death Bcl-2 family proteins, connects the death receptor and mitochondria apoptosis pathways. Cell research. 2000;10(3):161-7.

44. El Rayes SM, Ali IA, Fathalla W, Mahmoud MA. Synthesis and Biological Activities of Some New Benzotriazinone Derivatives Based on Molecular Docking; Promising HepG2 Liver Carcinoma Inhibitors. ACS omega. 2020;5(12):6781-91.

45. Dickson A, Tiwary P, Vashisth H. Kinetics of ligand binding through advanced computational approaches: a review. Current topics in medicinal chemistry. 2017;17(23):2626-41.

46. Hammad SG, El-Gazzar MG, Abutaleb NS, Li D, Ramming I, Shekhar A, et al. Synthesis and antimicrobial evaluation of new halogenated 1, 3-Thiazolidin-4-ones. Bioorganic chemistry. 2020;95:103517.

47. Anoop M, Binil P, Suma S, Sudarsanakumar M, Varghese HT, Panicker CY. Vibrational spectroscopic studies and computational study of ethyl methyl ketone thiosemicarbazone. Journal of Molecular Structure. 2010;969(1-3):48-54.

48. Mangalam NA, Kurup MP. Synthesis and spectral investigations of vanadium (IV/V) complexes derived from an ONS donor thiosemicarbazone ligand. Spectrochimica Acta Part A: Molecular and Biomolecular Spectroscopy. 2009;71(5):2040-4.

49. Ebrahimi S. Synthesis of some pyridyl and cyclohexyl substituted 1, 2, 4 triazole, 1, 3, 4-thiadiazole and 1, 3, 4-oxadiazole derivatives. European Journal of Chemistry. 2010;1(4):322-4.

50. Raj MM, Patel HV, Raj LM, Patel NK. SYNTHESIS AND BIOLOGICAL EVALUATION OF SOME NEW 1, 3, 4-THIADIAZOLE DERIVATIVES FOR THEIR ANTIMICROBIAL ACTIVITIES. International Journal of Pharmaceutical, Chemical & Biological Sciences. 2013;3(3).

51. Roeges NP, Baas J. A guide to the complete interpretation of infrared spectra of organic structures: Wiley New York; 1994.

52. Shyamsivappan S, Vivek R, Suresh T, Kaviyarasu A, Amsaveni S, Athimoolam S, et al. Novel Thiadiazoline Spiro Quinoline Analogues Induced Cell death in MCF-7 cells via G2/M Phase Cell Cycle Arrest. 2021.

53. Padmaja A, Pedamalakondaiah D, Sravya G, Reddy GM, Kumar MVJ. Synthesis and antioxidant activity of a new class of sulfone/sulfonamide-linked bis (oxadiazoles), bis (thiadiazoles), and bis (triazoles). Medicinal Chemistry Research. 2015;24(5):2011-20.

54. Kashtoh H, Hussain S, Khan A, Saad SM, Khan JA, Khan KM, et al. Oxadiazoles and thiadiazoles: novel α-glucosidase inhibitors. Bioorganic & medicinal chemistry. 2014;22(19):5454-65.

55. Blois MS. Antioxidant determinations by the use of a stable free radical. Nature. 1958;181(4617):1199-200.

56. AbdulJabar LA, AlShawi A, Mutlaq DZ. Anti-Liver and Anti-Breast Cancer Activities of Novel 2-Thioxo-4-Imidazolidinone Derivatives. 2021.

57. Mohammed MK, Al-Shuhaib Z, Al-Shawi AA. Synthesis, characterization and cytotoxicity appraisal of original 1, 2, 3-Triazole derivatives, against breast cancer cell lines (MDA-MB-231). Mediterranean Journal of Chemistry. 2019;9(4):305-10.

58. Al-Shawi AA, Hameed MF, Ali NH, Hussein KA. Investigations of phytoconstituents, antioxidant and anti-liver cancer activities of Saueda monoica Forssk extracted by microwave-assisted extraction. Asian Pacific Journal of Cancer Prevention: APJCP. 2020;21(8):2349.

59. Khan M, Yu B, Rasul A, Al Shawi A, Yi F, Yang H, et al. Jaceosidin induces apoptosis in U87 glioblastoma cells through G2/M phase arrest. Evidence-Based Complementary and Alternative Medicine. 2012;2012.

60. Wang Y, Zhao Y, Zhang A, Ma J, Wang Z, Zhang X. Targeting of miR-20a against CFLAR to potentiate TRAIL-induced apoptotic sensitivity in HepG2 cells. Eur Rev Med Pharmacol Sci. 2017;21(9):2087-97.

61. Jin Z, Wang Y, Yu X-F, Tan Q-Q, Liang S-S, Li T, et al. Structure-based virtual screening of influenza virus RNA polymerase inhibitors from natural compounds: molecular dynamics simulation and MM-GBSA calculation. Computational biology and chemistry. 2020;85:107241.

62. Lapierre J-M, Eathiraj S, Vensel D, Liu Y, Bull CO, Cornell-Kennon S, et al. Discovery of 3-(3-(4-(1-Aminocyclobutyl) phenyl)-5-phenyl-3 H-imidazo [4, 5-b] pyridin-2-yl) pyridin-2-amine (ARQ 092): An orally bioavailable, selective, and potent allosteric AKT inhibitor. Journal of medicinal chemistry. 2016;59(13):6455-69.

63. Day PJ, Cleasby A, Tickle IJ, O'Reilly M, Coyle JE, Holding FP, et al. Crystal structure of human CDK4 in complex with a D-type cyclin. Proceedings of the National Academy of Sciences. 2009;106(11):4166-70.

64. Chandrashekar DS, Bashel B, Balasubramanya SAH, Creighton CJ, Ponce-Rodriguez I, Chakravarthi BV, et al. UALCAN: a portal for facilitating tumor subgroup gene expression and survival

analyses. Neoplasia. 2017;19(8):649-58.

65. Li T, Fu J, Zeng Z, Cohen D, Li J, Chen Q, et al. TIMER2. 0 for analysis of tumor-infiltrating immune cells. Nucleic acids research. 2020;48(W1):W509-W14.

66. Li T, Fan J, Wang B, Traugh N, Chen Q, Liu JS, et al. TIMER: a web server for comprehensive analysis of tumor-infiltrating immune cells. Cancer research. 2017;77(21):e108-e10.

67. Santos A, Wernersson R, Jensen LJ. Cyclebase 3.0: a multi-organism database on cell-cycle regulation and phenotypes. Nucleic acids research. 2015;43(D1):D1140-D4.

Figures

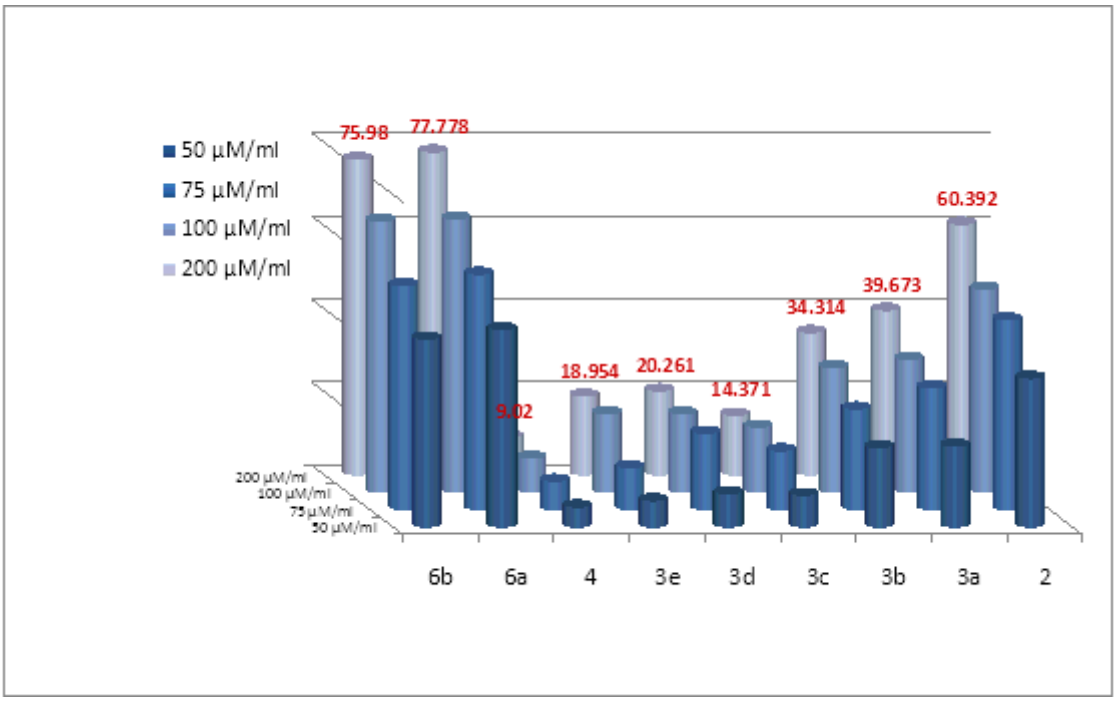

Figure 1

DPPH free radical scavenging activity of compounds (**2,3a,3b, 3c, 3d, 3e, 4, 6a,** and **6b**) at concentrations 50-200 µM showing the percentage of inhibition.

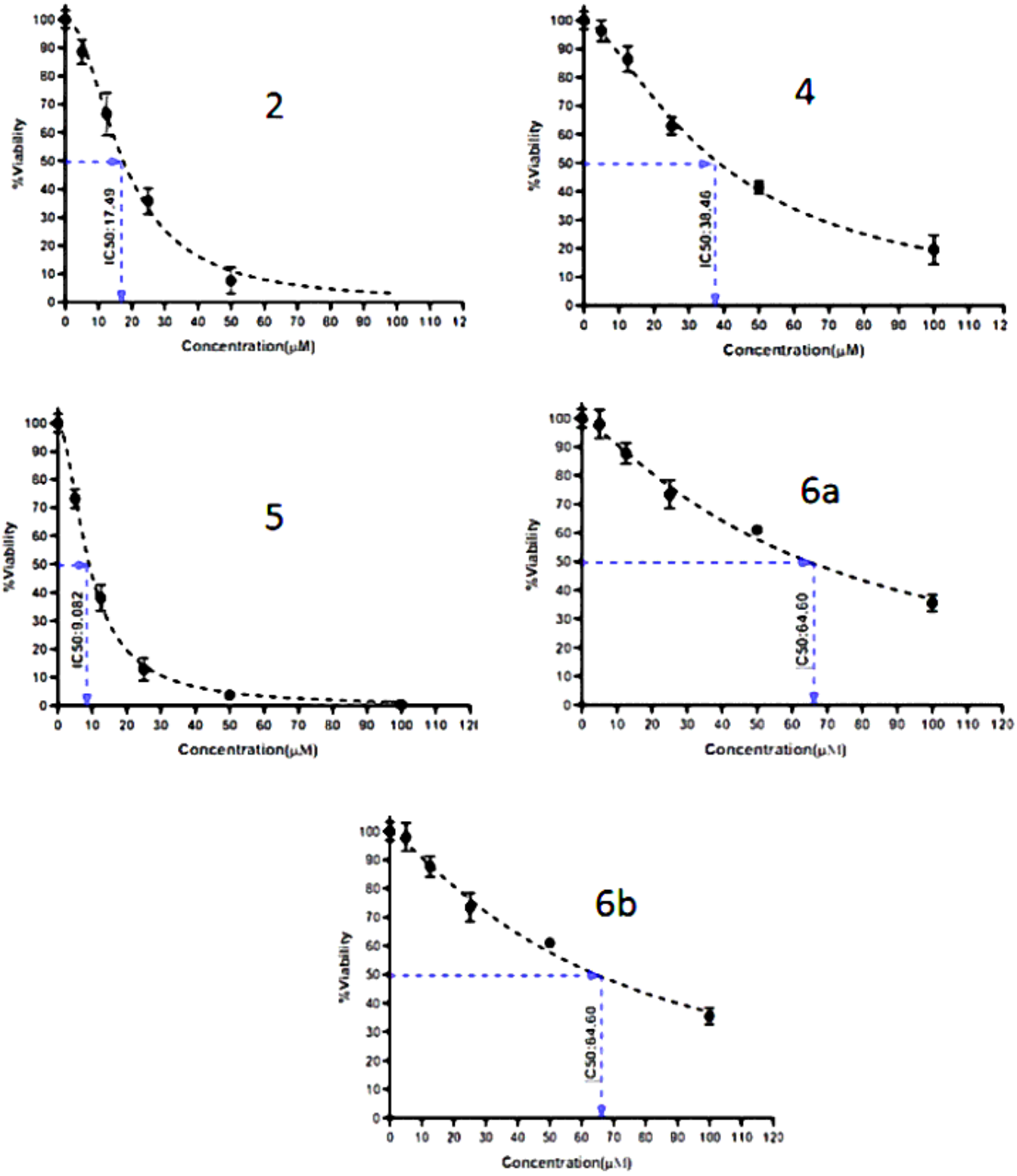

Figure 2

IC_{50} estimation of potential compounds (**2, 4, 5, 6a,** and **6b**)using MTT assay.

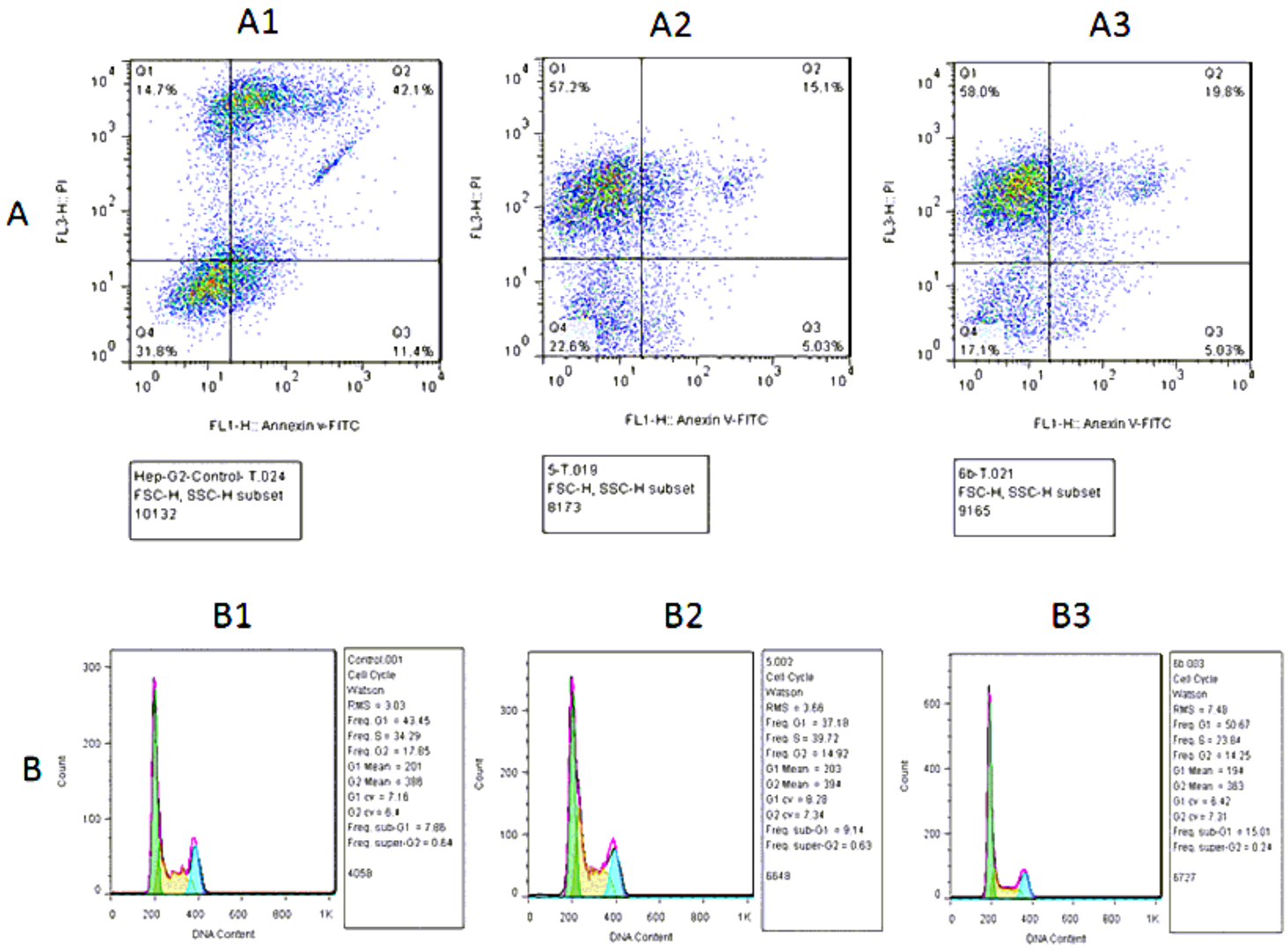

Figure 3

The flow cytometry analysis of **A**. Apoptosis analysis: **A1**. Untreated cells. **A2**. Cells treated with compound 5. **A3**. Cells treated with compound 6b. **B**. Cell cycle analysis: **B1**. Untreated cells. **B2**. Cells treated with compound 5. **B3**. Cells treated with compound 6b.

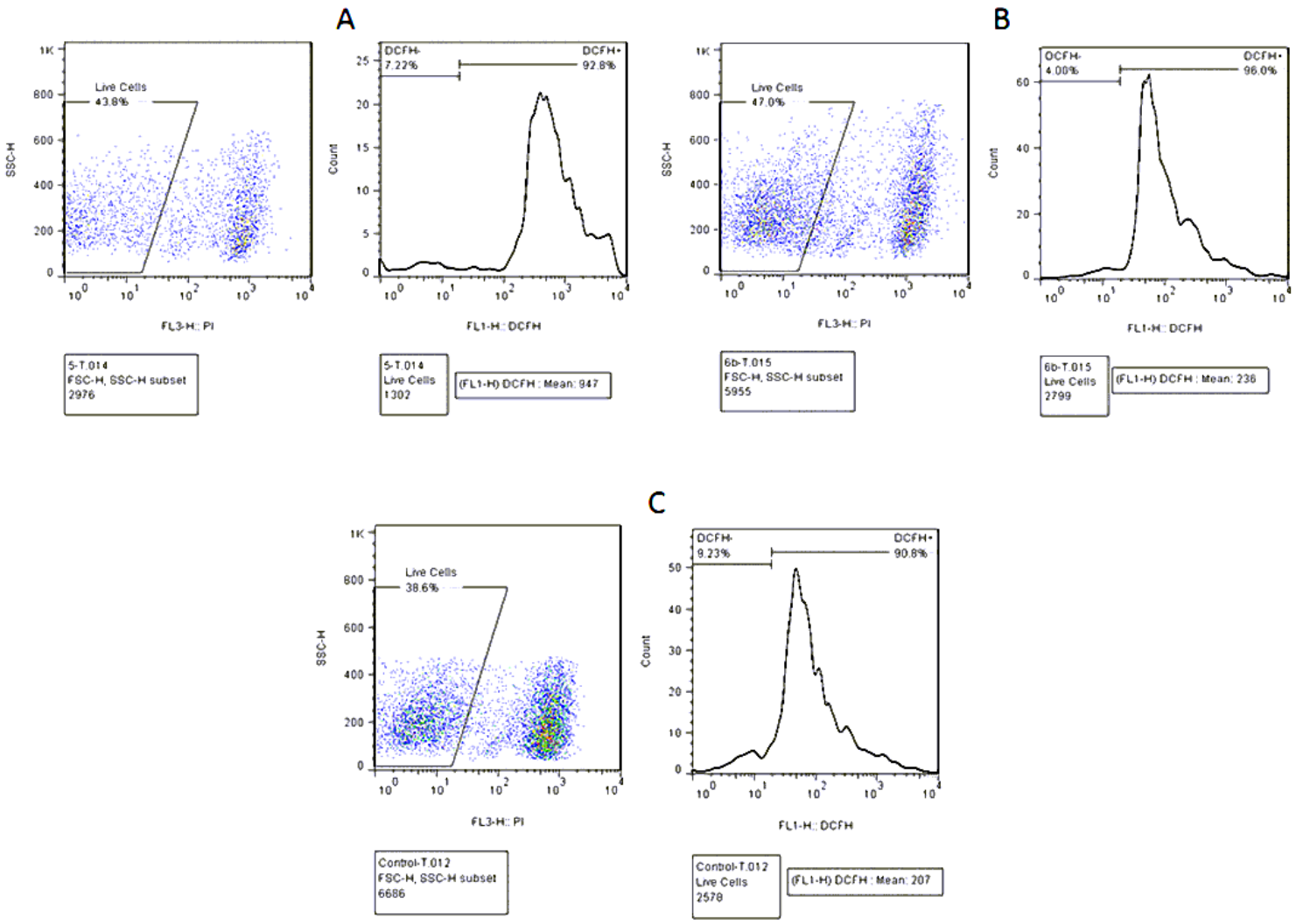

Figure 4

Flow cytometry analysis of reactive oxygen species: **A**. Cells treated with compound 5. **B**. Cells treated with compound 6b. **C**. Untreated cells.

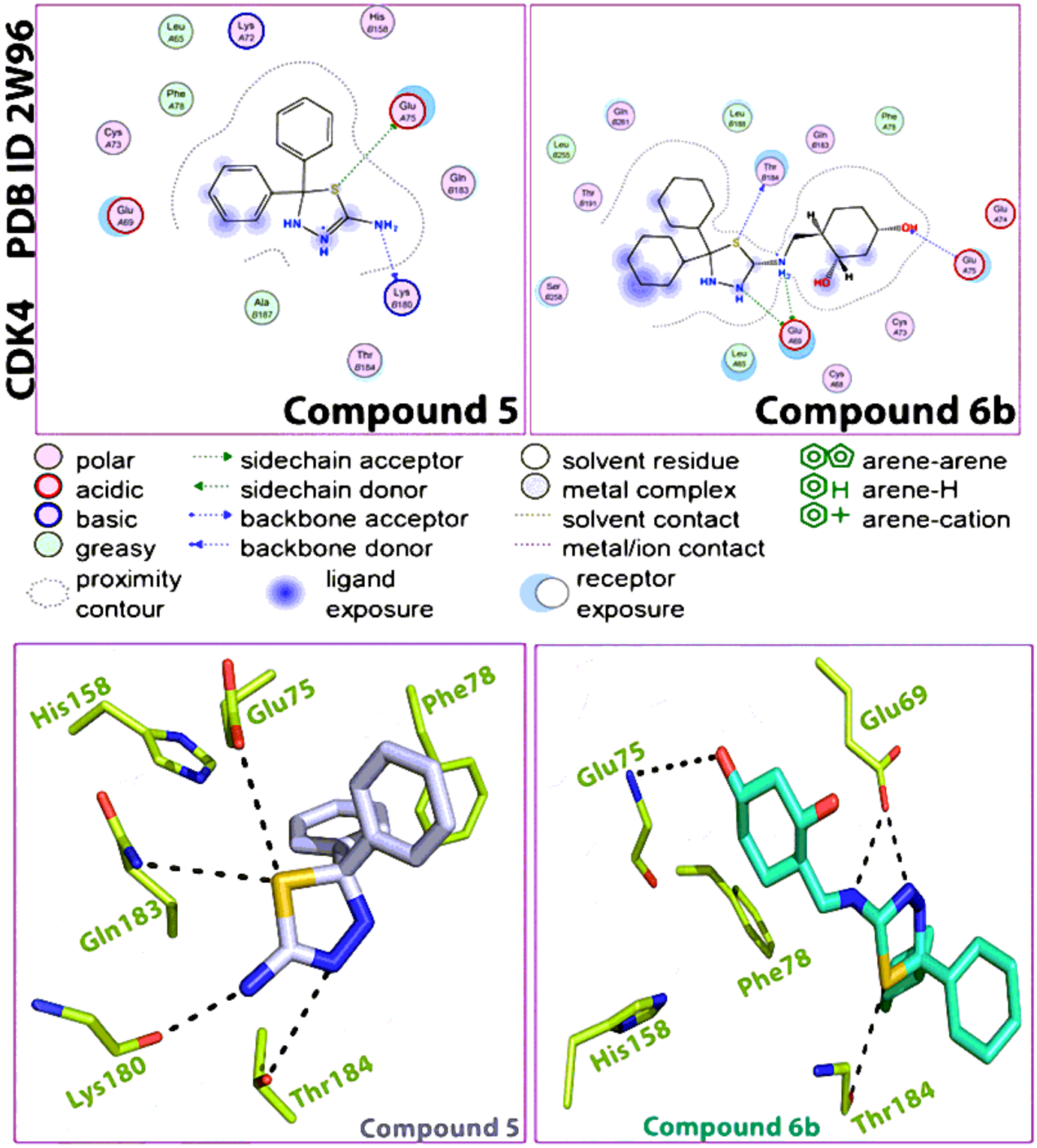

Figure 5

Flow cytometry analysis of reactive oxygen species: **A**. Cells treated with compound 5. **B**. Cells treated with compound 6b. **C**. Untreated cells.

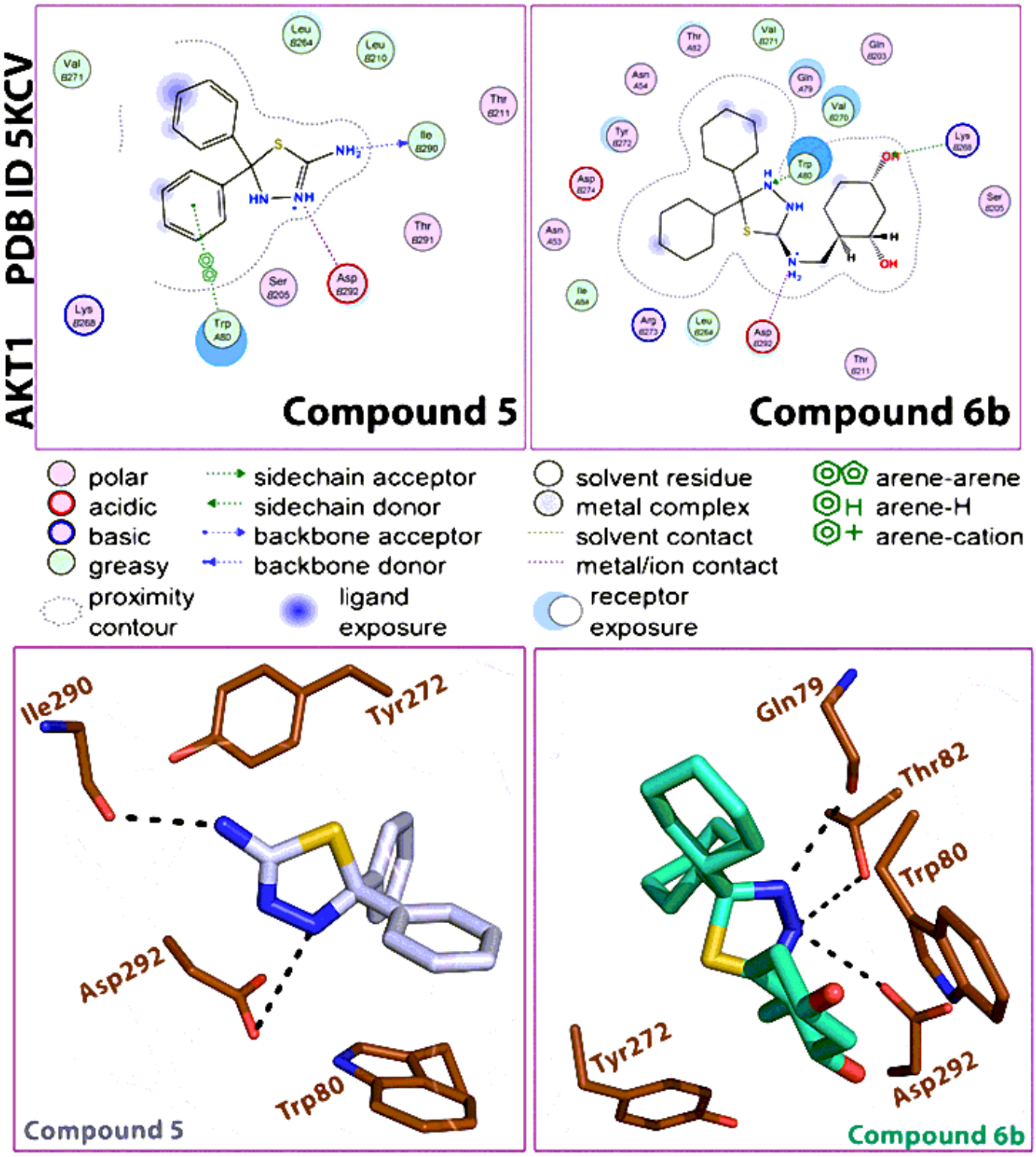

Figure 6

Two and three dimensional of compound 5 and 6b interaction with the active site of target protein Akt1 .

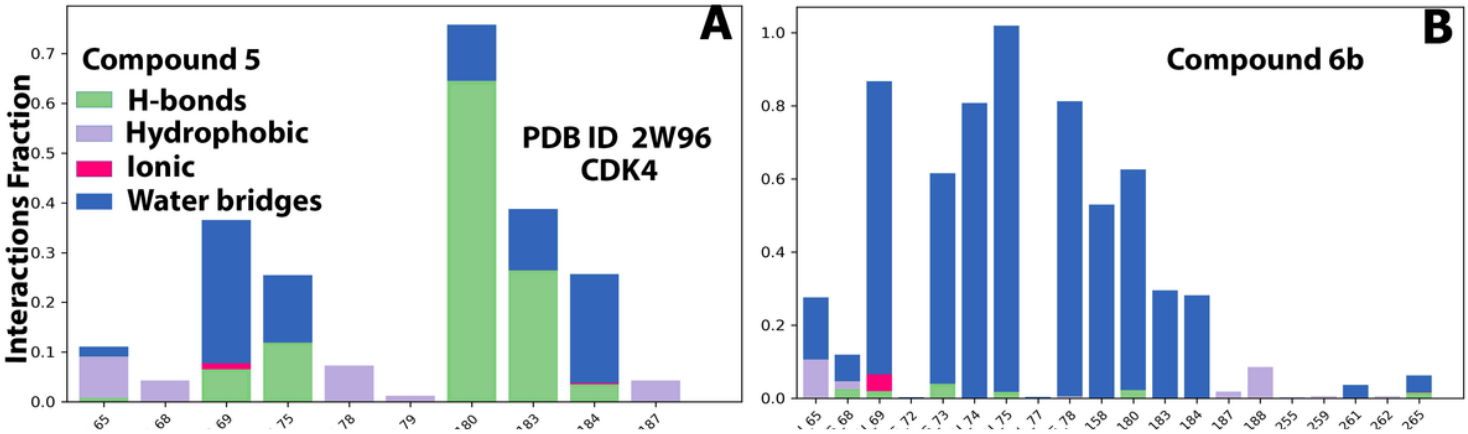

Figure 7

Throughout the trajectory, the bar charts depict protein-compound interaction,

(A) compound 5-CDK4-complex, (B)compound 6b-CDK4-complex, (C)compound 5-AKT1-complex , (D) compound 6b-AKT1-complex

Figure 8

Root Mean Square Deviation (RMSD) , (A) compound 5-CDK4-complex, (B)compound 6b-CDK4-complex, (C)compound 5-AKT1-complex , (D) compound 6b-AKT1-complex.

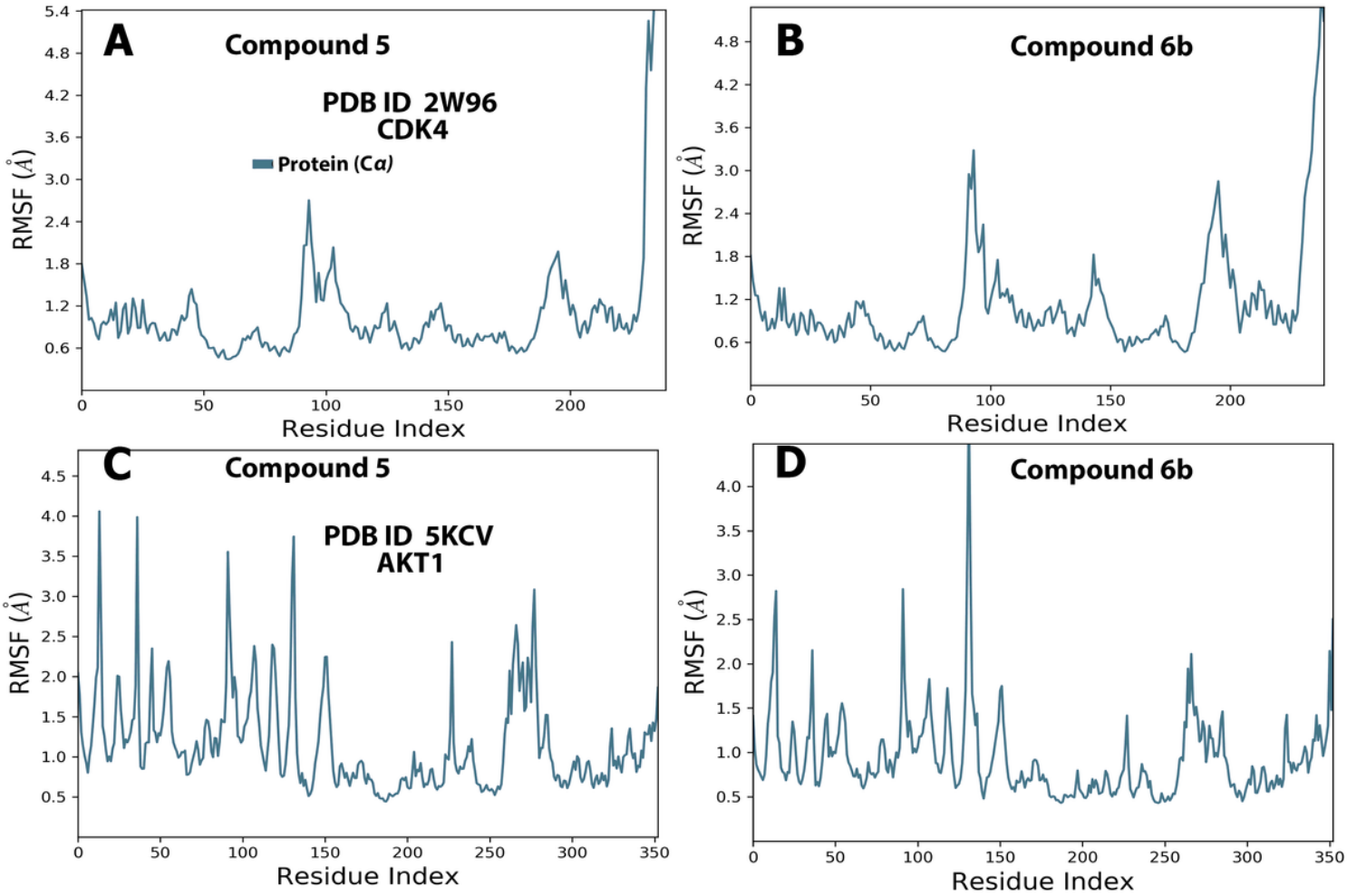

Figure 9

Root Mean Square Fluctuation (RMSF), (A) compound 5-CDK4-complex, (B)compound 6b-CDK4-complex, (C)compound 5-AKT1-complex , (D) compound 6b-AKT1-complex.

Figure 10

bioinformatic result for AKT1

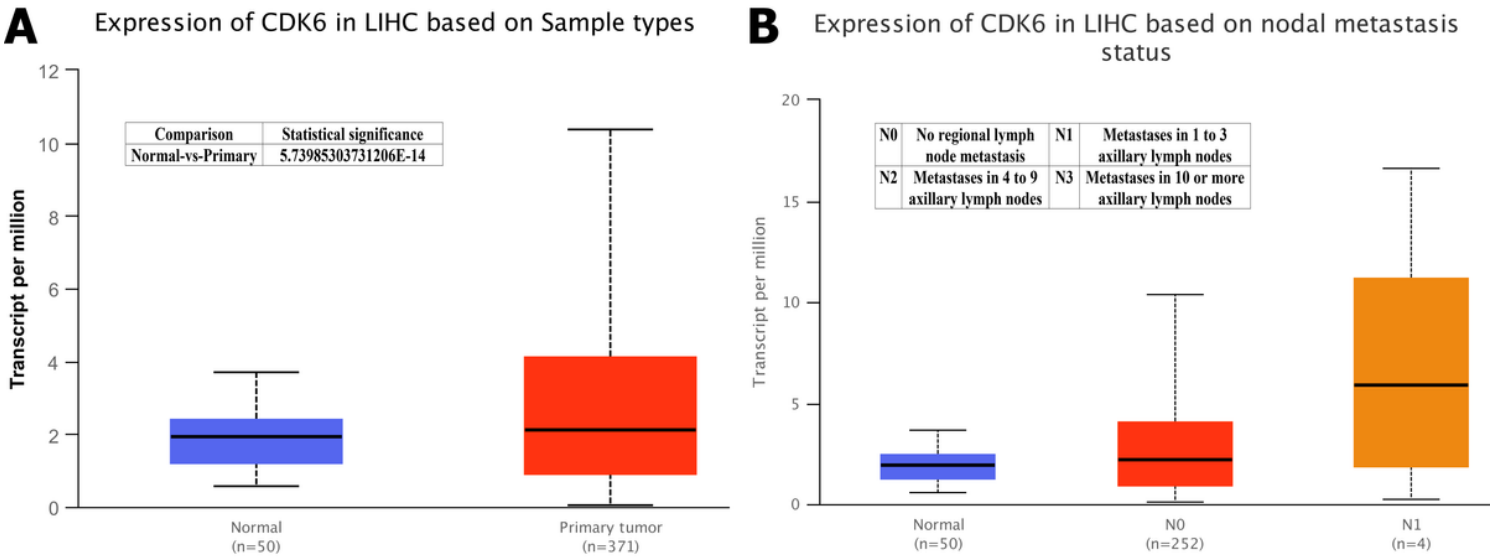

Figure 11

bioinformatic result for CDK6

Supplementary Files

This is a list of supplementary files associated with this preprint. Click to download.

- supplementarydataFTIRspectra.pdf
- supplementarydataHNMRspectra.pdf
- supplementarydatamassspectra.pdf
- supplementarydataofCNMRspectra.pdf